Bulgarian Chemical Communications, Volume 48, Special Issue E (pp. 199 - 205) 2016

Numerical simulation of latent heat storage with conductance enhancing fins

Nedžad R. Rudonja[1*], Mirko S. Komatina[1], Dragi Lj. Antonijević[2], Goran S. Živković[3]

1University of Belgrade, Faculty of Mechanical Engineering, Kraljice Marije 16, Belgrade, Serbia
2Faculty of Applied Ecology, Singidunum University, Požeška 83a, Belgrade, Serbia
[3]University of Belgrade, Institute of Nuclear Sciences "Vinča", Laboratory for Thermal Engineering and Energy, P.O. Box 522, 11001 Belgrade, Serbia

Precise understanding of heat transfer processes inside the latent thermal energy storage exposed to different initial and boundary conditions is crucial for development of optimized design and operating features of similar devices. The paper presents 3D numerical study of phase change material heat storage in the shape of vertical cylinder reservoir with axially placed heat source/sink equipped with variable number of conductance enhancing longitudinal rectangular fins. As the principally important observed is the case of vertically variable heat flux supplied to the phase change material during the melting process. The numerical modeling is based on the physical model of the process and is being carried out by Fluent software that uses finite volume method for solving continuity, momentum and energy equations. The coupling between pressure and velocity is based on the Semi-Implicit Pressure-Linked Equation (SIMPLE) algorithm. The results of numerical simulations are verified through the comparison with the own experimental results. Exemplary results for characteristic heat storage geometries and boundary conditions are presented and analyzed in the paper.

Keywords: thermal energy storage, phase change material, heat transfer fins, numerical simulation

INTRODUCTION

The thermal energy storages (TES) utilizing phase change materials are used for eliminating the mismatch between energy supply and energy demand as well as for reducing energy consumption, operational costs and environmental impacts. Commonly, the phase change materials (PCM) provide high energy storage densities, by nearly constant phase change temperatures [1, 2]. Furthermore, the organic PCM (e.g. paraffin), have identical melting and solidification curve [3]. Nevertheless, most of the PCMs have low values of thermal conductivity and therefore the prolonged times of melting and solidification. A simple and reliable way for overcoming the issue of low PCM thermal conductivity is utilization of metal fins [2, 4, 5].

An accurate understanding of heat transfer processes inside TES operated with various PCMs and exposed to different initial and boundary conditions is crucial for development of optimized design and operating features of similar devices. Since the analytical methods of solving melting and solidification problem are applicable only to the limited numbers of problems [6], the approach of numerical modeling and simulation is applied. In the previous studies of similar problems [7, 8, 9] the heat transfer enhancement of PCM heat storage is analyzed based on the fins number or certain geometric feature (height, diameter, length, etc.).

* To whom all correspondence should be sent:
nrudonja@gmail.com

This study presents an improved approach where the heat transfer enhancement and the heat transfer surface variations are correlated through introduced feature named *Finned surface ratio*.

PHYSICAL MODEL

The observed TES has the shape of vertical cylinder filled with the PCM (Fig. 1). The thermo–physical properties of the selected PCM - paraffin E53 (commercial grade wax), have been thoroughly determined and described previously [4].

Along the reservoir the heat source is placed axially. The heat source is represented by 2400 W electric heater (EH), placed inside the cylindrical steel shell with inner diameter of 54 mm and wall thickness of 3 mm. The shell is finned with longitudinal rectangular fins (160x500x3 mm) as shown in Fig.1. The height of the reservoir is 500 mm, and its inner diameter 400 mm.

The three cases were analyzed:

1. Steel shell without fins;
2. Steel shell finned with 6 longitudinal rectangular equidistant fins;
3. Steel shell finned with 12 longitudinal rectangular equidistant fins.

The tracking of heat transfer enhancement was carried out by finned surface ratio. The finned surface ratio is defined as the ratio of overall heat transfer surface area in contact with PCM in case with fins and in case of steel shell without fins, i.e. as follows:

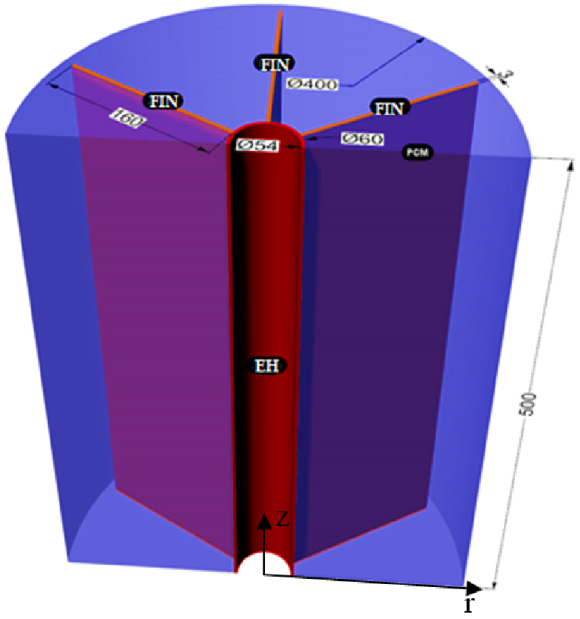

Fig.1. Cross section of TES physical model (case 2 - 6 longitudinal fins)

$$\gamma = \frac{n\left(2L_f Z_f + L_f \delta + 2Z_f \delta\right) + d\pi L_f - n\delta L_f}{d\pi L_f} \qquad (1)$$

where n is total number of fins (0, 6 or 12), L_f – fin length (500 mm), Z_f – fin height (160 mm), δ – fin thickness (3 mm), d – outer diameter of steel shell (60 mm). For the observed cases (1, 2 and 3), finned surface ratios calculated based on Eq.1. are: 1; 11.3 and 21.5.

ASSUMPTIONS

The following assumptions and simplifications have been made in order to enable mathematical description of transient heating and melting processes inside the three-dimensional physical model of the observed TES.

It has been assumed that the liquid phase of PCM behaves as non-compressible Newtonian fluid and that its flow inside the TES is laminar by character.

Further, the PCM enthalpy increase due to the viscous energy dissipation (PCM fluid phase internal friction) is neglected, as well as the heat transfer by thermal radiation inside the TES.

The joints between the cylindrical heater shell and the longitudinal fins have been considered ideal, i.e. the heat transfer contact resistance at the joints has been neglected.

The natural convection heat transfer in the liquid phase has been modeled using Businesq approximation, considering that the fluid density change is minimal.

The volume change due to the insertion of supplemental fins has been neglected (e.g. relative difference of PCM volume for the heat transfer surface with 6 fins and for the case without fins, amounts approximately 1.5%).

Finally, the heat flow through the outer walls of TES reservoir has been neglected, i.e. TES has been considered adiabatically insulated during the observed PCM melting process.

MATHEMATICAL MODEL

The physical model consists of three separate domains: domain of fin, domain of shell and domain of phase changing material. Since the domains of fin and shell remain in solid state during the observed processes, they could be well described by the energy equation in cylindrical (r, φ and z) coordinates (Fig.1):

$$\frac{\partial T}{\partial t} = \frac{\lambda}{\rho c_p}\left[\frac{1}{r}\frac{\partial}{\partial r}\left(r\frac{\partial T}{\partial r}\right) + \frac{1}{r^2}\frac{\partial^2 T}{\partial \varphi^2} + \frac{\partial^2 T}{\partial z^2}\right] \qquad (2)$$

where T, λ, ρ and c_p stand for temperature, thermal conductivity, density and specific heat capacity of shell and fin.

In order to fully describe the transient heat transfer and fluid flow processes in the domain of PCM, the system of mathematical model equations should be comprised of continuity equation (3), momentum equations (4-10), energy equation (11) and enthalpy-porosity equation (12). Enthalpy-porosity equation is part of technique introduced by Voller [10] where the melt interface is not tracked explicitly. Instead, the liquid fraction of the cell volume that is in liquid form is associated with each cell in the domain.

The continuity equation for the observed PCM domain is:

$$\frac{\partial u_r}{\partial r} + \frac{1}{r}\frac{\partial u_\varphi}{\partial \varphi} + \frac{\partial u_z}{\partial z} + \frac{u_r}{r} = 0 \qquad (3)$$

where u_r, u_φ and u_z are flow velocity components for the main directions of cylindrical coordinate system.

The momentum equations of the observed PCM domain, for the main directions of the cylindrical coordinate system are:

$$\rho\left[\frac{\partial u_r}{\partial t}+u_r\frac{\partial u_r}{\partial r}+\frac{u_\varphi}{r}\frac{\partial u_r}{\partial \varphi}-\frac{u_\varphi^{\,2}}{r}+u_z\frac{\partial u_r}{\partial z}\right]$$
$$=-\frac{\partial p}{\partial r}-\left[\begin{array}{l}\frac{1}{r}\frac{\partial\left(r\tau_{rr}\right)}{\partial r}+\frac{1}{r}\frac{\partial \tau_{r\varphi}}{\partial \varphi}\\ -\frac{\tau_{\varphi\varphi}}{r}+\frac{\partial \tau_{rz}}{\partial z}\end{array}\right]+S_r, \quad (4)$$

$$\rho\left[\begin{array}{l}\frac{\partial u_\varphi}{\partial t}+u_r\frac{\partial u_\varphi}{\partial r}+\frac{u_\varphi}{r}\frac{\partial u_\varphi}{\partial \varphi}\\ +\frac{u_r u_\varphi}{r}+u_z\frac{\partial u_\varphi}{\partial z}\end{array}\right]=$$
$$-\frac{1}{r}\frac{\partial p}{\partial \varphi}-\left[\begin{array}{l}\frac{1}{r^2}\frac{\partial\left(r^2\tau_{r\varphi}\right)}{\partial r}\\ +\frac{1}{r}\frac{\partial \tau_{\varphi\varphi}}{\partial \varphi}+\frac{\partial \tau_{\varphi z}}{\partial z}\end{array}\right]+S_\varphi. \quad (5)$$

$$\rho\left[\frac{\partial u_z}{\partial t}+u_r\frac{\partial u_z}{\partial r}+\frac{u_\varphi}{r}\frac{\partial u_z}{\partial \varphi}+u_z\frac{\partial u_z}{\partial z}\right]=$$
$$-\frac{\partial p}{\partial z}-\left[\frac{1}{r}\frac{\partial\left(r\tau_{rz}\right)}{\partial r}+\frac{1}{r}\frac{\partial \tau_{\varphi z}}{\partial \varphi}+\frac{\partial \tau_{zz}}{\partial z}\right] \quad (6)$$
$$+\frac{\rho g\beta_V\left(h-h_{ref}\right)}{c_p}+S_z,$$

where $\beta v = 0.000255\ K^{-1}$ is the thermal expansion coefficient, while h and h_{ref} are PCM enthalpies for certain temperature T, and for average PCM phase change temperature ($T_{ref} = 323\ K$), respectively. On this way the density variation with temperature was only considered in the body force term using the Boussinesq approximation to take into account the buoyancy effect (Eq.6.). The components of the viscous stress tensor in equations (4-6) are calculated as (7-8):

$$\tau_{rr}=-\mu\left[2\frac{\partial u_r}{\partial r}-\frac{2}{3}\left(\nabla\cdot\vec{u}\right)\right],$$
$$\tau_{\varphi\varphi}=-\mu\left[2\left(\frac{1}{r}\frac{\partial u_\varphi}{\partial \varphi}+\frac{u_r}{r}\right)-\frac{2}{3}\left(\nabla\cdot\vec{u}\right)\right], \quad (7)$$
$$\tau_{zz}=-\mu\left[2\frac{\partial u_z}{\partial z}-\frac{2}{3}\left(\nabla\cdot\vec{u}\right)\right].$$

$$\tau_{r\varphi}=\tau_{\varphi r}=-\mu\left[r\frac{\partial}{\partial r}\left(\frac{u_\varphi}{r}\right)+\frac{1}{r}\frac{\partial u_r}{\partial \varphi}\right],$$
$$\tau_{z\varphi}=\tau_{\varphi z}=-\mu\left[\frac{\partial u_\varphi}{\partial z}+\frac{1}{r}\frac{\partial u_z}{\partial \varphi}\right], \quad (8)$$
$$\tau_{zr}=\tau_{rz}=-\mu\left[\frac{\partial u_z}{\partial r}+\frac{\partial u_r}{\partial z}\right],$$

where μ is dynamic viscosity of PCM.

The additional pressure drop due to the liquid flow through the porous media [10] can be calculated for the main directions of cylindrical coordinate system as:

$$S_r=-A_{mush}\frac{\left(1-x_m\right)^2}{x_m^{\,3}+\varepsilon}u_r,$$
$$S_\varphi=-A_{mush}\frac{\left(1-x_m\right)^2}{x_m^{\,3}+\varepsilon}u_\varphi, \quad (9)$$
$$S_z=-A_{mush}\frac{\left(1-x_m\right)^2}{x_m^{\,3}+\varepsilon}u_z,$$

where A_{mush} and ε are default values for porous area (*mushy zone*) constant (10^5) and small number (0.001) for preventing division by zero. The participation of liquid phase in total PCM mass (porosity) x_m is referred to as the lever rule as a function of actual temperature in the observed location and known liquidus and solidus temperatures (T_l and T_s) of PCM.

$$x_m=0,\ T<T_s,$$
$$x_m=\frac{T-T_s}{T_l-T_s},\ T_s<T<T_l, \quad (10)$$
$$x_m=1,\ T_l<T.$$

The energy equation for the observed PCM domain is:

$$\frac{\partial\left(\rho H\right)}{\partial t}+u_r\frac{\partial\left(\rho H\right)}{\partial r}+\frac{u_\varphi}{r}\frac{\partial\left(\rho H\right)}{\partial \varphi}$$
$$+u_z\frac{\partial\left(\rho H\right)}{\partial z}=\lambda\left[\begin{array}{l}\frac{1}{r}\frac{\partial}{\partial r}\left(r\frac{\partial T}{\partial r}\right)+\\ \frac{1}{r^2}\frac{\partial^2 T}{\partial \varphi^2}+\frac{\partial^2 T}{\partial z^2}\end{array}\right], \quad (11)$$

where H stands for enthalpy of PCM.

Finally, the system of equations closes with Brent-Voller [10] enthalpy-porosity equation that

characterizes the relation between PCM enthalpy and its porosity (defined as PCM liquid phase participation in total PCM mass):

$$H = h + \Delta H = h + x_m h_{sl}. \quad (12)$$

where h_{sl} is latent heat of fusion for the PCM melting at given temperature.

The boundary conditions defining the mathematical model integration domains are given for the surfaces shown in Fig.2.

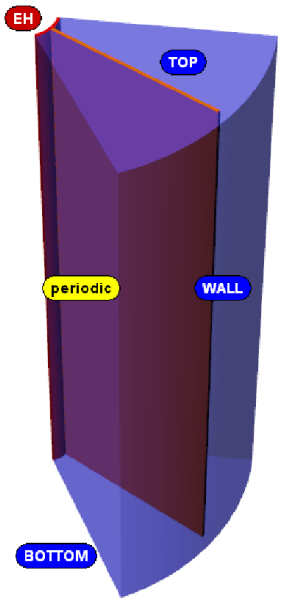

Fig.2. Boundary surfaces of the domains

Table 1. Initial and boundary conditions

	Initial	Boundary	Conditions
HEATER	T = 293 K	Top	$\dot{q} = 0$
		EH	$\dot{q}$ (Eqns.13)
		Bottom	$\dot{q} = 0$
PCM	T = 293 K	Top	$\mu \frac{\partial u_i}{\partial x_j} \approx 0$, $\dot{q} = 0$
	$\vec{u}$ = 0 m/s	Wall	$\vec{u} = 0$, $\dot{q} = 0$
		Bottom	$\vec{u} = 0$ $\dot{q} = 0$
		Periodic	Periodic b.c.
FINS	T = 293 K	Top	$\dot{q} = 0$
		Bottom	$\dot{q} = 0$

The boundary condition that describes the heat transfer process from the electrical heater to the PCM, at the surface of the steel shell, has been previously experimentally determined [4] as:

$$\dot{q} = 21000 - \frac{64000 \cdot (\exp(-5.322 \cdot z) - 1)}{5.322}, \quad (13)$$

where $\dot{q}$ is specific heat flux, and z axial coordinate as given in Fig.1.

The overview of the applied initial and boundary conditions for the performed calculations is given in Table1.

NUMERICAL SIMULATION

The proposed mathematical model is solved numerically by use of *FLUENT* software. The discretization of the mathematical model equations in this CFD program is based on the division of the defined domains into the finite number of control volumes (subdomains), effectuated through the appropriate mash generation, in which the value of the observed variables are calculated. The differential equations of the mathematical model (2-12) are integrated by time and volume for each of the control volumes.

The coupling between pressure and velocity was conducted by the Semi-Implicit Method for Pressure-Linked Equations (SIMPLE) algorithm [11]. The PRESTO scheme [11] was used for discretization of the pressure correction equation, while for the momentum and energy equations the first order upwind discretization scheme was used.

The time step of the utilized numerical scheme, proven by convergence testing, has been 1s. In total 200 iterations per time step provided convergence of the solutions.

The criteria for convergence of the numerical solutions were residual values of the considered equations, namely 10^{-4} for the continuity equation and the momentum equation, and 10^{-6} for the energy equation. The residual values as well as the values of utilized under-relaxation factors were determined based on the literature recommendations [12]. The values of under-relaxation factors for pressure, body force, momentum, density, energy and porosity, were: 0.3, 1.0, 0.2, 1.0, 1.0, and 0.9, respectively.

The values of thermophysical properties of the utilized PCM material (density ρ, specific heat capacity c_p, thermal conductivity λ, dynamic viscosity μ, solidus T_s and liquidus T_l temperatures and latent heat od fusion h_{sl}) as well as the properties of the other materials existing in subdomains (i.e. materials used for shell and fins), mandatory for the numerical solving of mathematical model equations, are listed in Table 2.

Table 2. Thermophysical characteristics of the utilized materials

Var.	Unit	PCM	Cu	Steel	Al
ρ	$\frac{kg}{m^3}$	842	8978	8030	2719
c_p	$\frac{J}{kgK}$	3000	381	502.48	871
λ	$\frac{W}{mK}$	0.36 *s* 0.91 *s-l* 0.18 *l*	387.6	16.27	202.4
μ	Pas	0.005	–	–	–
T_s	K	313	–	–	–
T_l	K	333	–	–	–
h_{sl}	$\frac{J}{kg}$	155881	–	–	–

NUMERICAL RESULTS

The numerical calculations have been performed for the three cases of physical model. In order to speed up the simulations, axial symmetry of the observed cases has been used, i.e. only one radial cut of the domain have been analyzed. For example, the temperature distribution in PCM, in case of the heating surface geometry with 6 longitudinal fins, after 60 min of heat supply is shown in Fig.3, whilst Fig.4 shows temperature distribution for the same case after 120 min of heating.

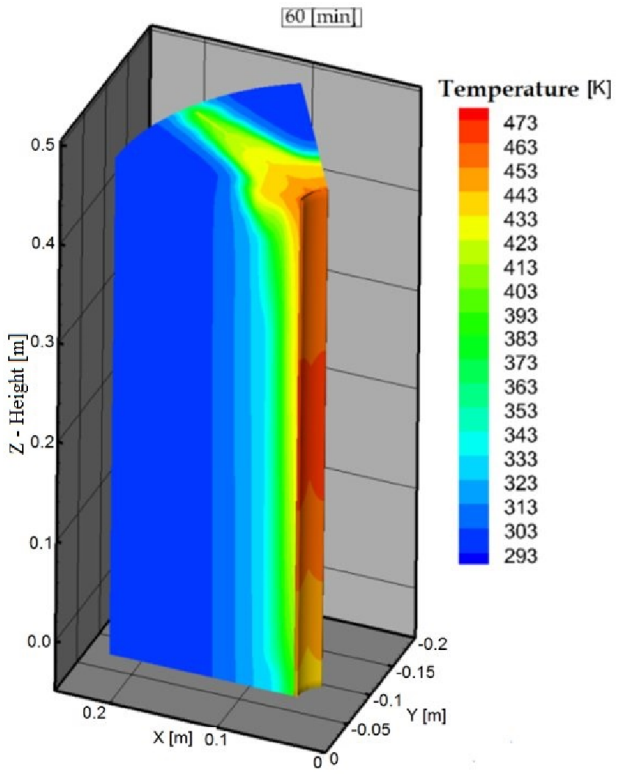

Fig.3. Temperature field inside TES with 6 fins after 60min of heating

The results of extensive numerical simulations, performed for the observed TES geometries, enabled derivation of functional dependences of heat transfer surface area (represented by dimensionless finned surface ratio) and time needed for full PCM melting by various initial and boundary conditions.

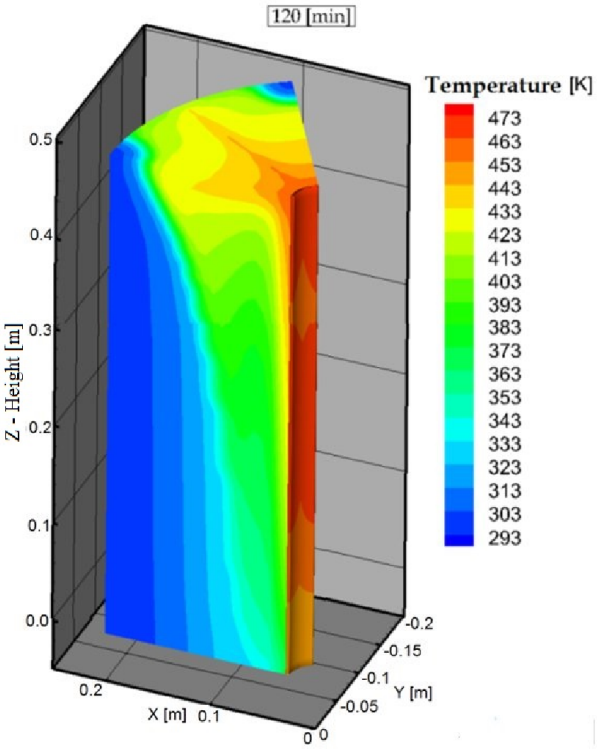

Fig.4. Temperature filled inside TES with 6 fins after 120min of heating

An example of such dependence, for copper fins, and initial and boundary conditions given in Table 1, is shown in Fig.5. It is noticeable that increasing the heat transfer surface, by adding the longitudinal rectangular fins to the heater, improves the heat transfer in TES and substantially decreases overall PCM melting time. Compared to the finless shell, adding of 6 fins, with the given geometry ($\gamma = 11.3$), accelerates the PCM melting approximately 4.4 times, i.e. the overall melting time amounts 22.7% of the melting time with finless heater (in the case of the same heat flux supplied to the PCM). In case of 12 fins ($\gamma = 21.5$) the heat transfer is expectedly further improved, and overall melting time amounts only 12% of the time needed in the case of finless heater.

In order to examine the influence of the applied fin material on the process of heating and melting of PCM, the simulations have been performed with three different fin materials: copper, steel and aluminum (Table 2). Increased fin material thermal conductivity contributes significantly to the heat

flow in radial direction, enabling higher temperatures of the fin towards the fin tips and thus supplying more heat to the further radial zones of the cylindrical PCM reservoir. For example, by the boundary and initial conditions given in Table 1, utilization of copper fins provides a relative decrease of overall melting time of 49.4% compared to steel fins, and of 8.6% compared to aluminum fins of the same shape, number and size (Fig.6).

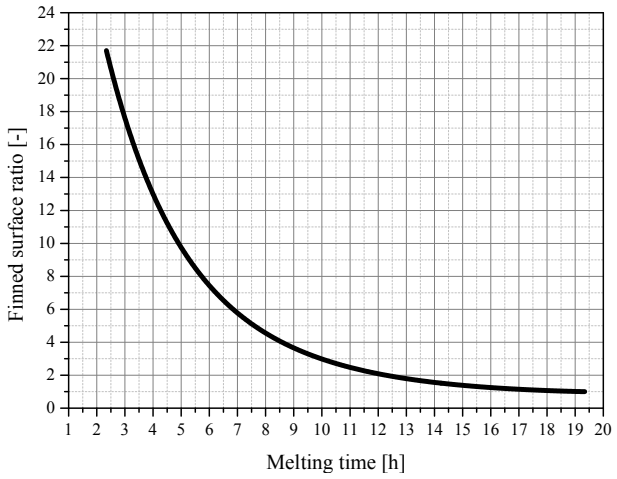

Fig.5. Dependence of PCM melting time upon heat transfer surface area (Finned surface ratio)

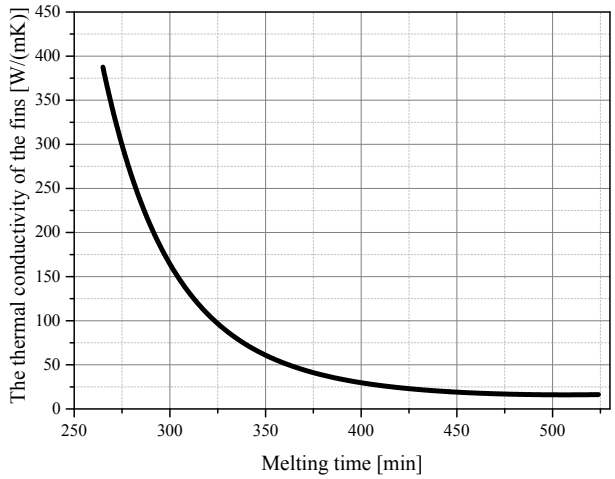

Fig.6. Dependence of PCM melting time upon thermal conductivity of fin (the 6 fins TES)

EXPERIMENTAL VERIFICATION OF NUMERICAL RESULTS

In order to verify the results of numerical solving of the mathematical model, the comparison with the own experimental results is performed. The experimental investigations were performed at laboratory TES installation shown in Fig.7 and thoroughly described in [4].

Fig.7. Experimental installation

The experimental verification of the results is performed by observing and comparison of the PCM temperatures in several indicative locations of TES, during the melting process. For the illustration, the temperature readings of thermocouples, at locations B_2 *(r = 90 mm, z = 280 mm)* and C_2 *(r = 150 mm, z = 280 mm* are compared to the corresponding numerical results. The resemblance and conformity of the temperature curves derived experimentally and numerically is excellent (Fig.8 and Fig.9), both by their character overlapping and by the closeness of the absolute values during the process.

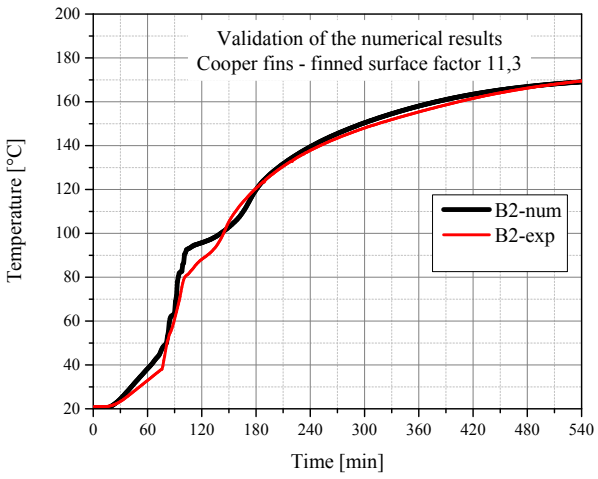

Fig.8. Temperature at location B_2 determined numerically and experimentally

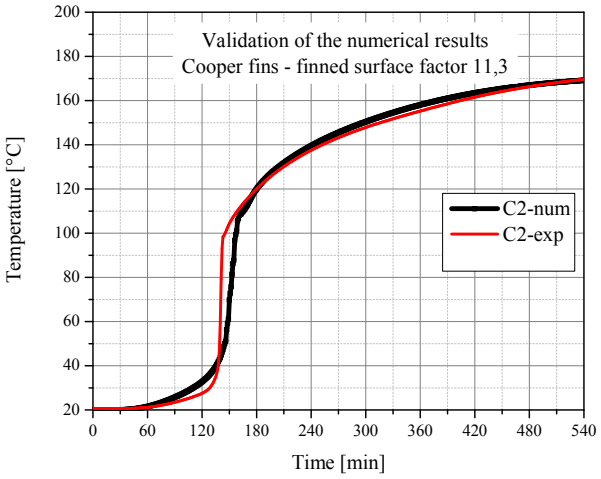

Fig.9. Temperature at location C_2 determined numerically and experimentally

CONCLUSION

The longitudinal rectangular fins attached to the axially placed heater of the cylindrical TES with PCM, have been used for reduction of the prevailing thermal resistances caused by low thermal conductance of paraffin and for the stimulation of PCM heating and melting.

The proposed mathematical model of the processes inside TES has been solved numerically and the results compared to the characteristic results obtained experimentally. For a sharpened observation of the interrelations between enlarged heat transfer surfaces and achieved process improvements, the dimensionless finned surface ratio has been introduced. It has been concluded that the overall melting time of PCM inside the TES, by the observed initial and boundary conditions, decrease exponentially with the finned surface ratio increase.

An excellent agreement between the results of PCM temperature change in the control locations obtained numerically and experimentally has been demonstrated. The experimental and numerical temperature curves almost overlap in most TES locations. Thus, it has been concluded that the proposed mathematical model and the numerical procedure can be implemented for analysis and calculations of heating and melting processes of a PCM of known thermophysical characteristics utilized within a cylindrical TES, with longitudinal rectangular fins, of various size and design.

ACKNOWLEDGMENT

The authors wish to thank the Ministry of Education, Science and Technological Development of Republic of Serbia, for financing projects III42011, TR 33042 and OI 176006.

REFERENCES

1 A. Waqas, Z. Ud Din, *Renewable and Sustainable Energy Reviews,* 18, 607 (2013).
2 K.A. Ismail, C.L.. Alves, and M.S. Modesto, *Applied Thermal Engineering* , 21, 53 (2001).
3 A. Lázaro, E. Günther, H. Mehling, S. Hiebler, J.M. Marín, B. Zalba, *Measurement Science and Technology*, 17, 2168 (2006).
4 N. Rudonja, M. Komatina, G. Zivkovic, D. Antonijevic, *Thermal Science,* 136 (2015).
5 T. Rozenfeld, Y. Kozak, R. Hayat, G. Ziskind, *International Journal of Heat and Mass Transfer,* 86, 465 (2015).
6 H.H. S.A. Argyropoulos, *Modelling and Simulation in Materials Science and Engineering,* 4, 371 (1996).
7 A.H. Mosaffa, F. Talati, M.A. Rosen, H.B. Tabrizi, *International Communications in Heat and Mass Transfer,* 39, 318 (2012).
8 A. Castell, C. Solé, M. Medrano, J. Roca, L.F. Cabeza, D. García, *Applied Thermal Engineering,* 28, 1676 (2008).
9 S. Mat, A.A. Al-Abidi, K. Sopian, M.Y. Sulaiman, A.T. Mohammad, *Energy Conversion and Management*, 74, 223 (2013).
10 A.D. Brent, V.R. Voller, and K.J. Reid, *Numerical Heat Transfer,* 13, 297 (1988).
11 S. Patankar, Numerical heat transfer and fluid flow, McGraw-Hill Book Company, (1980).
12 A.R. Darzi, M. Farhadi, and K. Sedighi, *Applied Mathematical Modelling*, 36, 4080 (2012).